Article

Corrugated Photoactive Thin Films for Flexible Strain Sensor

Donghyeon Ryu [1,*] and Alfred Mongare [2]

[1] Department of Mechanical Engineering, New Mexico Tech; donghyeon.ryu@nmt.edu
[2] Department of Mechanical Engineering, New Mexico Tech; alfred.mongare@student.nmt.edu
* Correspondence: donghyeon.ryu@nmt.edu; Tel.: +1-575-835-5199

Abstract: In this study, a flexible strain sensor is devised using corrugated poly(3-hexylthiophene) (P3HT) thin film. In the previous studies, the P3HT-based photoactive thin film was shown to generate direct current (DC) under broadband light, and the generated DC voltage varied with applied tensile strain. Yet, the mechanical resiliency and strain sensing range of the P3HT-based thin film strain sensor were limited due to relatively more brittle thin film constituent – poly(3,4-ethylenedioxythiophene)-polystyrene(sulfonate) (PEDOT:PSS) conductive thin film as a bottom electrode. To address this issue, it is aimed to design mechanically resilient strain sensor using corrugated thin film constituents. Buckling is induced to form corrugation in the thin films by applying pre-strain to the substrate, where the thin films are deposited, and releasing the pre-strain afterwards. It is known that corrugated thin film constituents exhibit different optical and electronic properties from non-corrugated ones. Therefore, to optimize design of the flexible strain sensor, it was studied to understand how the applied pre-strain and thickness of the PEDOT:PSS thin film affect the optical and electrical properties. Also, pre-strain effect on light absorptivity of the corrugated P3HT-based thin films was studied. In addition, strain effect was investigated on the optical and electrical properties of the corrugated thin film constituents. Finally, flexible strain sensors are fabricated by following the design guideline, which is suggested from the studies on the corrugated thin film constituents, and DC voltage strain sensing capability was validated. As a result, flexible strain sensor exhibited tensile strain sensing range up to 5% at frequency up to 15 Hz with maximum gage factor ~7.

Keywords: P3HT; PEDOT:PSS; flexible sensor; strain sensor; photoactive self-sensing thin films

---

1. Introduction

Flexible strain sensors are widely used in various applications (*e.g.*, biomedical devices, flexible displays, soft robotics, automobiles, and aerospace structures, among many others). Unlike conventional strain sensors, the flexible strain sensors exhibit extended range of strain measurement as well as mechanical resiliency. To accomplish the design goal to devise flexible strain sensors, researchers have proposed various approaches by designing materials and sensing composites [1-5], modifying physical configurations [6,7], and patterning brittle components [8,9]. While the state-of-the-arts have showcased very impressive sensing capability and mechanical resiliency, majority of the flexible sensors are relied on piezoresistivity of sensing materials. These piezoresistive flexible strain sensors have intrinsic limitations, such as energy dependency and singular sensing mode, among some others.

To overcome the intrinsic limitations of the piezoresistive strain sensors, researchers have studied to suggest novel flexible strain sensor technologies [2,10-19]. Piezoelectric materials-based strain sensors showed impressive strain sensing performance [13,14]. It was reported that piezoelectric

Preprints (www.preprints.org) | NOT PEER-REVIEWED | Posted: 10 September 2018 doi:10.20944/preprints201809.0154.v1

Peer-reviewed version available at Materials 2018, 11, 1970; doi:10.3390/ma11101970

(1-x)Pb($Mg_{1/3}Nb_{2/3}$)O_3-xPbTiO_3 nanowire-based elastomeric composites generated electric voltage, which exhibited linear relationship with applied tensile strain, when exposed to tensile strain [14]. Mechanoluminescent (ML)-based elastomeric composites exhibited strains sensing capability based change in ML light intensity as well as color of light emission under tensile or compressive strains [15-18]. It was reported that ML copper-doped zinc sulfide (ZnS:Cu) micro-particles embedded in elastomeric matrix generated ML light under tension, of which luminescence showed linear relation with applied tensile strain up to ~35%, under tensile loading and unloading cycles [17]. These new classes of flexible strain sensing composites present promising prospects with multifunctional capabilities of energy conversion from mechanical energy to electrical energy or radiant energy.

Multifunctional mechano-luminescence-optoelectronic (MLO) composites were proposed to sense tensile strain using direct current (DC) voltage generated from the MLO composites under cyclic tensile loading and unloading [11,20]. The MLO composites consist of two functional components, such as mechano-optoelectronic (MO) poly(3-hexthylthiophene) (P3HT)-based thin film sensor and ML ZnS:Cu-embedded elastomeric composites. On one hand, it was shown that the MO P3HT-based thin film sensor generated DC current under light, which varied with applied tensile strain [21-23]. This MO P3HT-based thin film sensor's DC-based strain sensing capability did not require external electrical energy with gage factor of 2 or higher when carbon nanotube is doped into the P3HT-based sensing thin films. On the other hand, ML ZnS:Cu-based elastomeric composites, which is another functional component of MLO composites, emit light in response to mechanical stimuli [15]. Accordingly, the MLO composites are designed to measure strain using DC voltage output as a sensor signal via mechanical-radiant-electrical energy conversion. Nevertheless, the MLO composites-based strain sensor did not show large range of tensile strain sensing mainly due to cracks occurring in brittle constituents. In particular, the top and bottom electrodes developed cracks under strain above 1%. It is critical to make flexible MO P3HT-based strain sensor for improving strain sensing range and mechanical resilience of the MLO composites.

In this study, it is proposed to induce buckling in the thin film constituents of the flexible strain sensor consisting of corrugated functional thin films. Also, the brittle aluminum top electrode (*i.e.*, cathode) will be replaced with gallium-indium eutectic (EGaIn). The thin film constituents to be designed in form of corrugated thin films are a poly(3,4-ethylenedioxythiophene)-poly(styrenesulfonate) (PEDOT:PSS) thin film bottom electrode (*i.e.*, anode) and a P3HT-based self-sensing thin film. The bottom PEDOT:PSS thin film electrode is required to be electrically conductive and translucent thin film so that it can play a role as a bottom electrode to allow light through the thin film. The self-sensing thin film is fabricated with MO P3HT and [6,6]-phenyl-C61-butyric acid methyl ester (PCBM) semiconducting polymers to exhibit multifunctional capability of radiant-electrical energy conversion and DC-based strain sensing based on strain-sensitive light absorptivity.

It is aimed to suggest design guideline for the corrugated PEDOT:PSS and P3HT:PCBM thin film constituents for devising the flexible strain sensor. First, the corrugated PEDOT:PSS thin film will be characterized with various pre-strains and various numbers of layers to fabricate conductive and translucent bottom electrode. Second, the effect of pre-strain will be studied on the light absorptivity of the corrugated P3HT-based thin films under tensile strains. Last, the flexible strain sensor's strain sensing capability will be validated by measuring DC voltage under broadband light, which is generated from the sensor subjected to tensile loading and unloading cycles.

2. Experiment Details

2.1. Materials

P3HT (regioregularity = 93 – 95%; Mw = 50 – 70 kDa) and amorphous PCBM were purchased from Solaris Chem. PEDOT:PSS (product number: PH1000) was acquired from Heraeus Inc. Polydimethylsiloxane (PDMS; product number: Sylgard 184 kit) was obtained from Dow Corning. Fluoro surfactant (product number: FS-30) was purchased from Capstone. EGaIn and Dimethyl

Preprints (www.preprints.org) | NOT PEER-REVIEWED | Posted: 10 September 2018 doi:10.20944/preprints201809.0154.v1

Peer-reviewed version available at *Materials* **2018**, *11*, 1970; doi:10.3390/ma11101970

sulfoxide (DMSO) were purchased from Sigma-Aldrich. Other chemicals used in this study were obtained from Fisher Scientific.

2.2. Preparation of test specimens

2.2.1. Corrugated PEDOT:PSS conductive thin films

A total of 23 corrugated PEDOT:PSS thin films were prepared by varying pre-strain and the number of PEDOT:PSS thin film layers. Each test specimen is named as shown in Table 1. On one hand, six different pre-strains (*i.e.*, 1%, 3%, 5%, 10%, 15%, and 20%) were used to fabricate the corrugated thin film to exhibit different thin film buckling characteristics. On the other hand, five different thicknesses of PEDOT:PSS thin film were prepared by varying deposited number of PEDOT:PSS layers from 1 to 9 layers with 2-layer interval. For each test case, one corrugated PEDOT:PSS conductive thin film specimen was prepared.

The fabrication procedure began from preparation of PEDOT:PSS conductive dispersion. 100 ml of conductive PEDOT:PSS dispersion was prepared by blending the PH1000, DMSO, and fluoro surfactant. 5 ml of DMSO was added to 95 ml of PH1000, and the PH1000 and DMSO blend was manually agitated to homogenize the blend. Then, 11 drops of fluoro surfactant were added to the PH1000 and DMSO blend and manually stirred. To eliminate any possible agglomeration of PEDOT:PSS, the conductive PEDOT:PSS dispersion was filtered using 0.45 μm polyvinylidene fluoride (PVDF) filter.

PDMS substrates were prepared on 100 mm diameter silicon wafers. First, silicon wafers were cleaned using isopropyl alcohol (IPA) and dried with compressed air. Second, PDMS mixture was prepared by blending 10 g of silicon base (PDMS I) and 1g of curing agent (PDMS II) and manually stirring it with a glass rod for 2 min. The PDMS mixture was degassed under vacuum in the desiccator for 1 hour. Third, the degassed PDMS was poured over the clean silicon wafer with extra caution not to entrap any air bubbles into the PDMS casted on silicon wafer. The PDMS casted silicon wafer was transferred to the vacuum oven to anneal at 80 °C for 2 h to crosslink the PDMS. The disk-shape PDMS substrate (diameter = 100 mm and thickness = 1 mm) was carefully removed from the silicon wafer. Then, rectangular PDMS substrates (length = 75 mm and width = 12.5 mm) were cut from the disk-shape PDMS substrate.

The rectangular PDMS substrate was pre-strained by manually stretching the PDMS substrate to the desired magnitude of tensile strain and fixed onto a glass slides (length = 75 mm and width = 25 mm) with two paper clips. Air bubbles at the interface between the PDMS substrate and the glass slides were carefully removed by rubbing the PDMS surface with nitrile-gloved finger. The pre-strained PDMS substrate was cleaned again with IPA and then dried with compressed air. Lastly, the pre-strained PDMS substrate was treated with UV ozone cleaner for 2 h to improve wettability of the PDMS substrate.

Table 1. Corrugated PEDOT:PSS conductive thin films specimens are named according to pre-strain and the number of layers.

Pre-strain [%] / Number of layers	1	3	5	10	15	20
1	P1L1	P3L1	P5L1	P10L1	P15L1	P20L1
3	P1L3	P3L3	P5L3	P10L3	P15L3	P20L3
5	P1L5	P3L5	P5L5	P10L5	P15L5	
7	P1L7	P3L7	P5L7			
9	P1L9	P3L9	P5L9			

Preprints (www.preprints.org) | NOT PEER-REVIEWED | Posted: 10 September 2018 doi:10.20944/preprints201809.0154.v1

Peer-reviewed version available at Materials 2018, 11, 1970; doi:10.3390/ma11101970

Table 2. Corrugated P3HT:PCBM photoactive thin film specimens are named according to pre-strain level.

Number of layers \ Pre-strain [%]	1	3	5	10	15	20
1	P1	P3	P5	P10	P15	P20

The pre-strained PEDOT:PSS thin film on the glass slide was mounted in the spin coater immediately after the UV ozone cleaning process is completed. The conductive PEDOT:PSS dispersion was dispensed over the entire area of the pre-strained PDMS substrate after filtering using 0.45 μm pore-size PVDF filter membrane. Spin-process began by spreading the PEDOT:PSS dispersion at 300 revolutions per minute (rpm) for 50 s, during which spin speed was linearly increased from 0 to 300 rpm for 10 s and maintained at 300 rpm for 40 s. Consequently, the conductive EDOT:PSS thin film was coated by spinning at 750 rpm for 30 s. To dry out moisture from the PEDOT:PSS thin film, spinning continued by increasing the speed to 1,000 rpm for 15 s and maintaining 1,000 rpm for 2 min. The deposited PEDOT:PSS thin film was annealed in a vacuum oven at 100 °C for 10 minutes. This process completed one layer deposition of the conductive PEDOT:PSS thin film. Specimens having more than one layer were fabricated by repeating the process for the subsequent PEDOT:PSS layer after cooling the thin film for 2.5 min.

2.2.2. Corrugated P3HT:PCBM photoactive thin films

To fabricated corrugated P3HT:PCBM photoactive thin film, P3HT:PCBM solution was prepared. 1:1 w./v.% P3HT:PCBM photoactive solution was prepared by dissolving P3HT and PCBM in dichlorobenzene (DCB). First, 3 w./v.% P3HT and 3 w./v.% PCBM solutions were prepared by dissolving 0.15 g of P3HT and 0.15 g of PCBM in each 5 ml of DCB, respectively. The solutions were heated at 45 °C and stirred at 450 rpm for 72 h. To minimize degradation of the solutions, vials containing the solutions were wrapped with paraffin film and aluminum. Then, the solutions were cooled to room temperature and filtered using 0.45 μm polytetrafluoroethylene (PTFE) filter membrane to remove possible agglomerates. To produce 1:1 w./v.% P3HT:PCBM photoactive solution, the 3 w./ v.% P3HT, PCBM solutions, and DCB were blended by 1:1:1 by volume and manually agitated.

The corrugated P3HT:PCBM photoactive thin films were deposited onto pre-strained PDMS substrates (length = 75 mm and width = 12.5 mm). A total of six P3HT:PCBM thin film specimens were prepared with only single layer at six different pre-strain levels of 1, 3, 5, 10, 15, and 20% (Table 2). The prepared 1:1 w./v.% P3HT:PCBM solution was dispensed, after filtering using 0.45 μm PTFE membrane, uniformly over entire area of the PDMS substrate. Then, deposition process by spin-coating technique began. Spin-coating of P3HT:PCBM photoactive thin films was performed using a similar spread and spinning program used for deposition of PEDOT:PSS thin films. Only one difference is shorter spinning duration for 1 min, instead of 2 min, in the last step at 1,000 rpm. The deposited P3HT:PCBM thin films were annealed in a vacuum oven. It should be noted that the P3HT:PCBM thin film was covered with a petri dish to retard evaporation of DCB during annealing process, which enhances optoelectronic properties of the P3HT:PCBM. Then, the specimen was annealed at 110 °C for 1 h.

2.2.3. Flexible thin film strain sensor

A total of six flexible strain sensors were fabricated by varying the number of PEDOT:PSS layers and pre-strain applied onto the pre-strained PDMS substrates (length = 75 mm and width = 12.5 mm) (Table 3). The sensor fabrication procedure (Figure 1a) began from deposition of PEDOT:PSS conductive thin films onto the pre-strained PDMS substrate by following same methodology described in 2.2.1. Once the desired number of PEDOT:PSS layers (*i.e.*, 7 or 9 layers) were deposited, a single layer of P3HT:PCBM photoactive thin film was coated onto the PEDOT:PSS layers by

Preprints (www.preprints.org) | NOT PEER-REVIEWED | Posted: 10 September 2018 doi:10.20944/preprints201809.0154.v1

Peer-reviewed version available at Materials 2018, 11, 1970; doi:10.3390/ma11101970

Table 3. Flexible strain sensors are named according to pre-strain and the number of PEDOT:PSS conductive thin films.

Pre-strain [%] / Number of PEDO:PSS layers	1	3	5
7	FS-P1L7	FS-P3L7	FS-P5L7
9	FS-P1L9	FS-P3L9	FS-P5L9

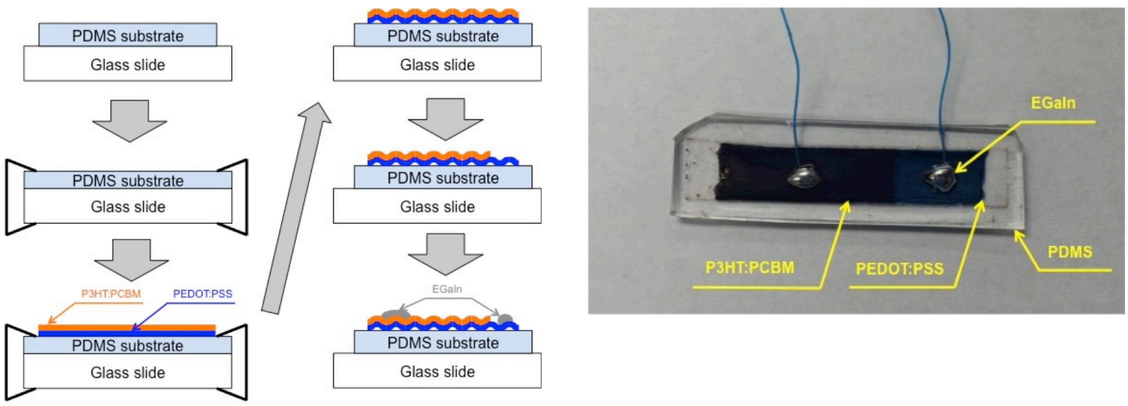

(a) (b)

Figure 1. (a) Flexible strain sensor is fabricated by inducing buckling in P3HT:PCBM and PEDOT:PSS thin film constituents by pre-straining the PDMS substrate. (b) A fabricated strain sensor is shown from top view.

following same procedure shown in 2.2.2. Then, one end of the coated P3HT:PCBM thin films was cleaned with DCB to expose a rectangular area (length = 20 mm and width = 12.5 mm), which is for establishing an electrical connection onto the conductive PEDOT:PSS thin films. Then, two electrical connections were made onto the exposed PEDOT:PSS thin films and onto the P3HT:PCBM thin films using EGaIn and 30 American wire gage (AWG) wires. By releasing the PDMS substrate after removing the paper clips, the deposited PEDOT:PSS and P3HT:PCBM thin films are naturally corrugated to produce flexible strain sensor with liquid EGaIn top electrode (*i.e.*, cathode).

The completed flexible strain sensors with the electrical wires were encased in PDMS to minimize environmental effect and hold the electrical wire connections in place. The flexible strain sensors were placed a 100 mm diameter petri dish. Wires of the sensors were attached to the edge of the petri dish using a glue gun not to disturb the EGaIn electrical connections during PDMS casting. Then, 22 g of degassed PDMS mixture was prepared and carefully poured into the petri dish to prevent air bubbles from being entrapped during casting. The PDMS encasing was cross-linked by annealing in a vacuum oven at 80 °C for 2 h. Finally, the flexible strain sensor specimens were prepared after carving out the specimens from the PDMS encased sensors (Figure 1b).

2.3. Test setup

2.3.1. Characterization of optical transmittance of PEDOT:PSS at tensile strains

The corrugated PEDOT:PSS thin films were interrogated with an ultraviolet-visible (UV-Vis) spectrophotometer to acquire an optical transmittance spectrum in the wavelength range from 300 to 900 nm. Eleven different UV-Vis transmittance spectrums were acquired at eleven different tensile strain levels during loading from 0% to a maximum strain, which is pre-strain applied for fabrication of the PEDOT:PSS specimen, and unloading back to 0% strain using a custom-built load frame (Figure 2). The specimens were strained by loading in five steps and unloaded in equal five steps by releasing the strain. One step is one fifth of the pre-strain or maximum applied tensile

Preprints (www.preprints.org) | NOT PEER-REVIEWED | Posted: 10 September 2018 doi:10.20944/preprints201809.0154.v1
Peer-reviewed version available at *Materials* **2018**, *11*, 1970; doi:10.3390/ma11101970

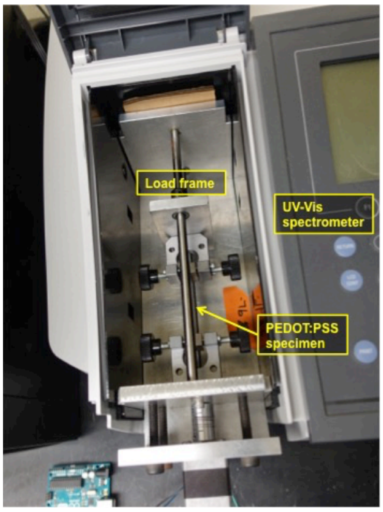

Figure 2. UV-Vis spectrophotometer equipped with a custom-built load frame, which fits in measurement chamber of the UV-Vis spectrophotometer, is used for measuring optical spectrum of test specimens at various strain levels.

strain. So, a total of eleven UV-Vis transmittance spectrums were produced from one set of testing with one specimen.

2.3.2. Characterization of sheet resistance of PEDOT:PSS at tensile strains

To measure sheet resistance of the corrugated PEDOT:PSS thin films, two electrodes were established on the thin films using copper tape and silver paste as shown in inset of Figure 3. Two straps of copper tapes wrapped near two ends of the PEDOT:PSS thin films specimen while maintaining a distance larger than 25 mm between the copper tapes. Then, silver paste was applied at the margin of copper tape to ensure electrical connections between copper tape and PEDOT:PSS thin films. Inner edges of the silver pasted areas were distanced 25 mm, which was used when calculating sheet resistance as an initial length at 0% strain. The length used to calculate sheet resistance was changed when the specimen was stretched. Width of the thin film to calculate sheet resistance was 12.5 mm, which did not change with varying strain.

A digital multimeter (DMM; product number: Keithley 2450) was used to measure four-point probed resistance at various strains. Strain was applied using the custom-built load frame shown in Figure 3. Like optical transmittance characterization test, eleven strains were applied to the PEDOT:PSS thin film specimens during one cycle of loading and unloading. So, a total of 11 resistance were obtained and used for calculating using:

$$Sheet\ ressitance = (Measured\ resistance \times Width)/Length \tag{1}$$

Among 23 specimens, only 15 specimens, which have more than one layer, were tested by varying strain. Please note that two specimens (*i.e.*, 15p5l and 20p3l) failed during testing. Sheet resistances were also measured for the rest of specimens with single PEDOT:PSS layer but only at 0% without straining those specimens using the load frame.

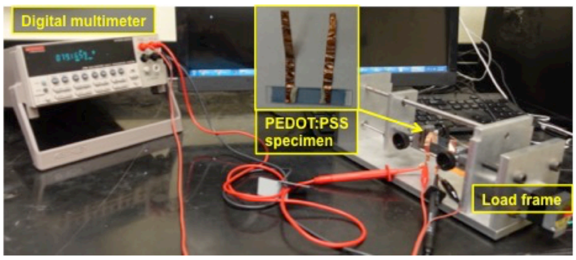

Figure 3. Electrodes were established on the corrugated PEDOT:PSS thin film specimen to measure four-point probed resistance using digital multimeter at various tensile strains.

Peer-reviewed version available at Materials 2018, 11, 1970; doi:10.3390/ma11101970

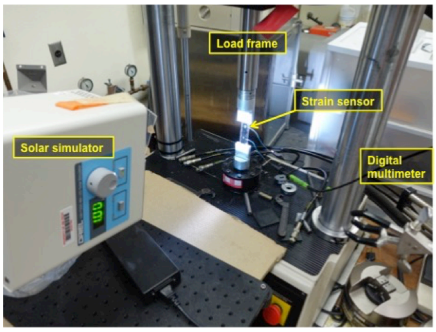

Figure 4. The flexible strain sensor was tested to validate its DC voltage-based strain sensing capability under tensile loading and unloading cycles while measuring DC voltage under one-sun light.

2.3.3. Characterization of light absorption of P3HT:PCBM at tensile strains

A test setup for characterization of UV-Vis light absorptivity of the P3HT:PCBM photoactive thin films specimen is identical to the test setup shown in Figure 2 for optical transmittance characterization of the PEDOT:PSS thin film specimens. Instead of transmittance, the measurement mode for the P3HT:PCBM thin film specimen is light absorption spectrum from 300 nm to 900 nm wavelength.

2.3.4. Validation of strain sensing of high flexible thin films strain sensor

The fabricated flexible strain sensors first were subjected to quality test by measuring current-voltage (IV) responses using a source-measurement unit (SMU; product number: Keithley 2450) under one-sun light from a solar simulator (product name: Oriel 7320 LED solar simulator) and without light. Then, qualified strain sensors were tested for strain sensing validation using the test setup shown in Figure 4. To apply cyclic tensile loading and unloading to the flexible strain sensor, a servo-hydraulic load frame was used. DC voltage was measured from the sensor using the digital multimeter under one-sun light from the solar simulator. The testing room was maintained as dark as possible to minimize effect by ambient light.

3. Results and Discussion

3.1. Optical transmittance of PEDOT:PSS at tensile strains

Figure 5 shows four representative light transmittance spectrums that were acquired at six different tensile strains during loading cycle to clearly present how the transmittance changes with strain. It should be noted that the light transmittance during unloading exhibited similar trend with applied tensile strain. By comparing transmittance from 1% pre-strain specimens shown in Figure 5a and b to the results from 15% pre-strain specimens shown in Figure 5c and d, one can understand that overall transmittance of the specimen fabricated at 1% is higher than the transmittance of the specimen prepared at 15% pre-strain. In addition, it can be seen that, as there are more number of layers, overall transmittance decreases by comparing the Figure 5a and c to Figure 5b and d. Also, the overall transmittance increases as the tensile strain applied to the specimen increases, which is shown clearly in Figure 5c and d due to strain applied up to 15%.

To better understand how pre-strain, at which the specimens were fabricated, affects transmittance, peak transmittance was obtained from each transmittance spectrum at 0% strain from each test specimen (Figure 6a). The peak transmittance at 0% strain shows decreasing trend as the pre-strain increases up to 15% while it increases again when pre-strain is 20% compared to 15% case. The specimens with 7 and 9 layers of PEDOT:PSS thin films exhibit different characteristics from the other specimens with less number of layers (*i.e.*, 1, 3, and 5 layers). Those large number (*i.e.*, 7 and 9

Preprints (www.preprints.org) | NOT PEER-REVIEWED | Posted: 10 September 2018 doi:10.20944/preprints201809.0154.v1

Peer-reviewed version available at *Materials* **2018**, *11*, 1970; doi:10.3390/ma11101970

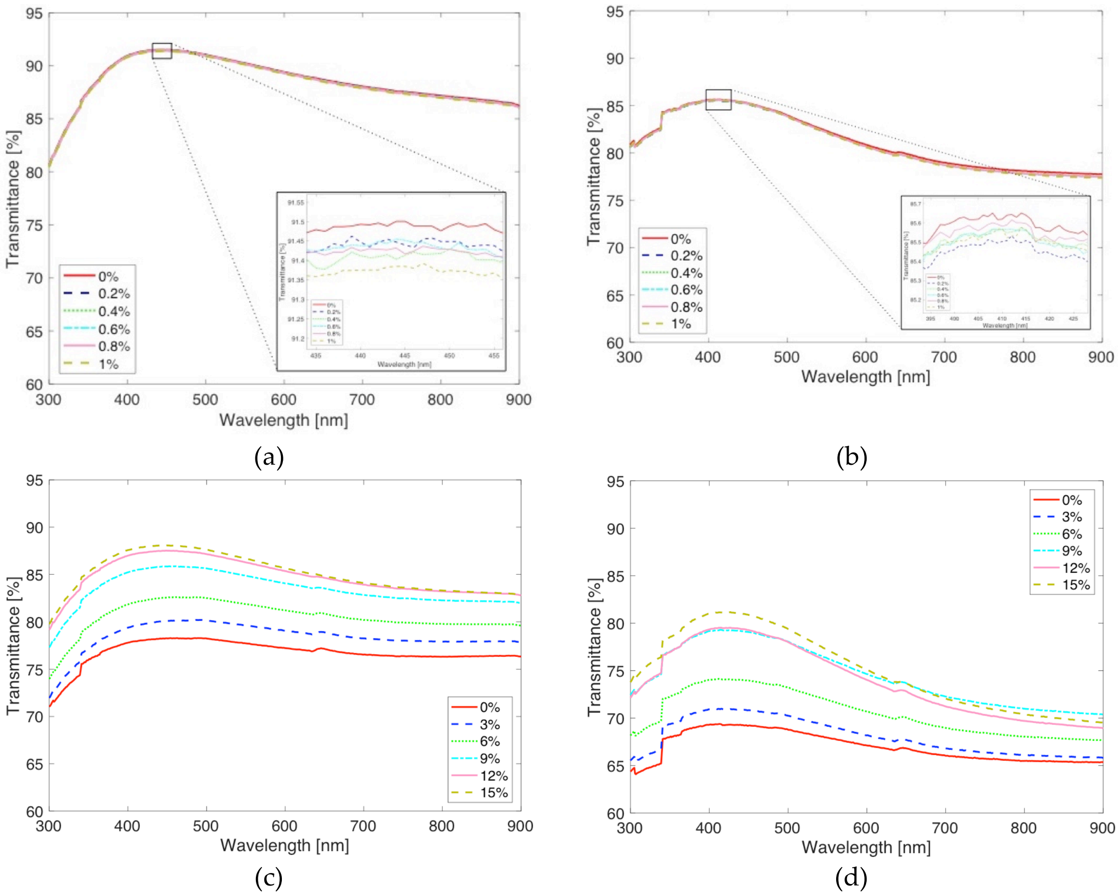

Figure 5. Light transmittance spectrums are shown from (a) 1P1L and (b) 1P9L during loading from 0% to 1% tensile strain; and (c) 15P1L and (d) 15P5L during loading from 0% to 15% tensile strain.

layers) of layer specimens' peak transmittance decreases from 1% to 3% pre-strain but increases again from 3% to 5% strain. The decreasing transmittance trend with increasing pre-strain from a specimen having a constant number of PEDOT:PSS layer seems mainly due to wrinkles formed in the corrugated thin films. Six specimens having three layers, which were fabricated at six different pre-strains, were observed using an optical microscope (Figure 6b). Wrinkles are shown in all 6 specimens. But, for the three specimens fabricated at low pre-strain (*i.e.*, 1%, 3%, and 5%), depth of wrinkles as well as density of wrinkles are smaller than ones in other specimens prepared at higher pre-strain (*i.e.*, 10%, 15%, and 20%). So, peak transmittances at 0% strain for higher pre-strain specimens are larger than lower pre-strain specimens' transmittance due to more populated and deeper wrinkles. This is because the higher pre-strain exceeded critical buckling strain of the PEDOT:PSS thin film while smaller pre-strain was not large enough to induce buckling. Up to 15% pre-strain, since more wrinkles and deeper wrinkles are formed as pre-strain increases, peak transmittance decreases as the pre-strain increases. However, peak transmittance increases again from 15% to 20% for both 1 layer and 3 layers specimens, which is even higher than the peak transmittance at 10% pre-strain. This seems due to shallower or less wrinkles in 20% specimens compared to 10% and 15% specimens. On the other hand, peak transmittance of specimens having larger number of layers decreases when pre-strain increases from 1% to 3% pre-strain but increases again when pre-strain increases from 3% to 5%. While 3P7L and 5P7L specimens show similar number of wrinkles in the limited viewfinder in Figure 6c, wrinkles in 5P7L seem to be a little shallower than the ones in 3P7L, which could result in higher peak transmittance at higher pre-strain.

The peak transmittance data are plotted differently to study the effect of the number of layers on the peak transmittance (Figure 7a). The corrugated PEDOT:PSS thin films, which were fabricated at

Peer-reviewed version available at Materials 2018, 11, 1970; doi:10.3390/ma11101970

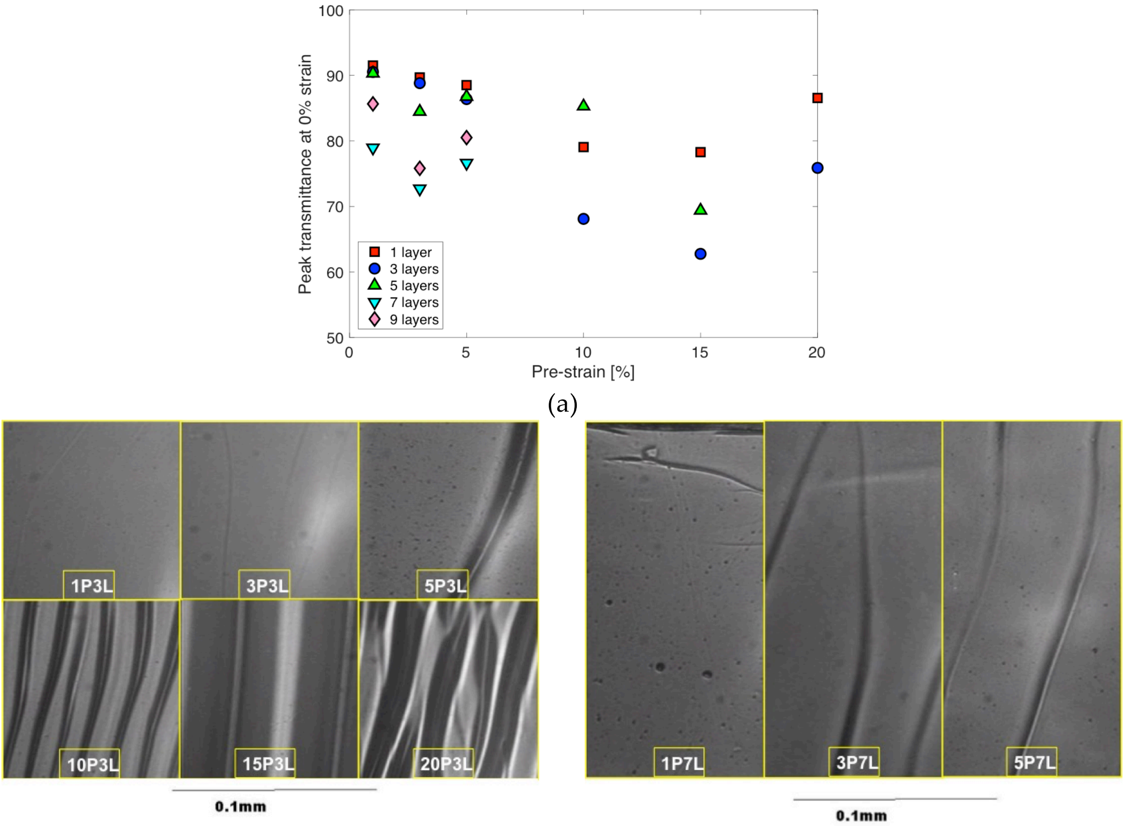

(a)

(b) (c)

Figure 6. (a) Peak transmittances at 0% strain are shown with pre-strain that was applied when fabricating corrugated PEDOT:PSS thin film specimens. Optical microscopic images are shown for the corrugated thin films having (b) 3 layers and (c) 7 layers.

low pre-strain (*i.e.*, 1%, 3%, and 5%), exhibit similar trend of peak transmittance change with the number of layers. Up to 5 layers, change in peak transmittance was small. As the number of layer increases from 5 to 7, peak transmittance shows sharp decreases. At 9 layers, the peak transmittance increases again. It was shown that, for non-corrugated PEDOT:PSS thin films, peak transmittance decreased with increasing number of layer (*i.e.*, increasing thickness of thin film), which could be explained by Beer-Lambert law [24]. However, the corrugated PEDOT:PSS thin films show non-linear behavior, which can be thought due to optical effect by the wrinkles in the corrugated thin films. To qualitatively investigate the wrinkles' effect on the optical transmittance, optical microscopic images of 5% pre-strain specimens were taken and shown in Figure 7b. One can see that wrinkles' depth decreases as the number of layers increases up to 5 layers. The consistent light transmittance up to 5 layer specimens seems to results from cancelling effect by the lower wrinkle profiles at larger number of layers. Thicker thin films (*i.e.*, thin films with larger number of layer) are expected to have higher critical strain against thin film buckling, which results in formation of shallower wrinkles. The sharp decrease in transmittance from 5 to 7 layers seems due to increasing thickness as well as increased depth of wrinkles. Increased peak transmittance of the 9 layer specimen could result from the smaller number of wrinkles formed in the thin films. On the other hand, high pre-strain specimens show different characteristics in peak transmittance. The representative 10% pre-strain specimens' optical microscopic images are shown in Figure 7c. Comparing 1 layer and 3 layer specimens, there are more wrinkles with deeper profiles in 3 layer specimen, which results in decrease of peak transmittance. When the number of layer increased from 3 to 5, the peak transmittance increased gain due to lower dense of wrinkles.

Peer-reviewed version available at Materials 2018, 11, 1970; doi:10.3390/ma11101970

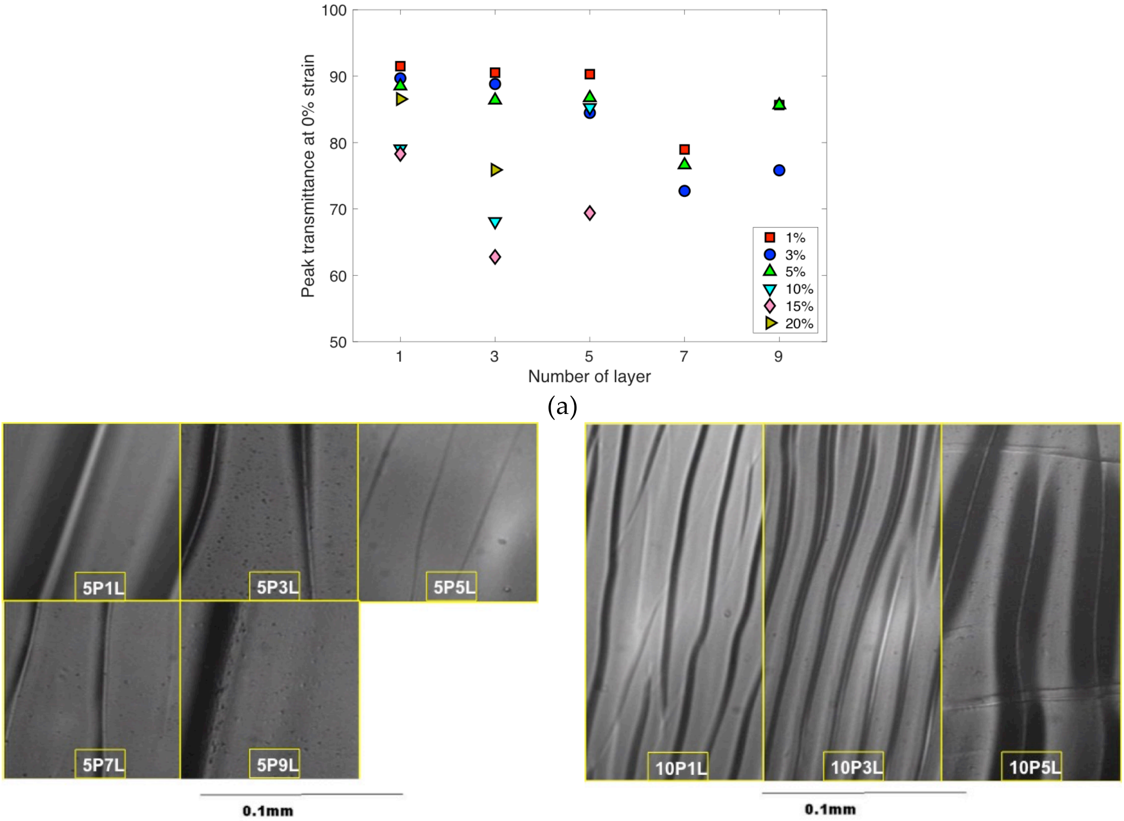

(a) (b) (c)

Figure 7. (a) Peak transmittances at 0% strain are shown with the number of PEDOT:PSS layers. Optical microscopic images are shown for the corrugated thin films that were fabricated at (b) 5% pre-strain and (c) 10% pre-strain.

In addition, to understand the effect of tensile strain applied to the corrugated PEDOT:PSS thin films on the light transmittance, peak transmittance acquired at each of the applied tensile strains was normalized using:

$$T_{NP} = \left(T_P - T_{P,0\%}\right)/T_{P,0\%} \tag{2}$$

where, T_{NP} is normalized peak transmittance, T_P is peak transmittance at a strain, $T_{P,0\%}$ is peak transmittance at 0% strain. The normalized peak transmittance is shown with the applied tensile strain in Figure 8. Assuming that the corrugated PEDOT:PSS thin films become more flat as higher strain is applied, one can think that light transmittance increases due to less optical interference. This trend is commonly observed in Figure 8a and b for small and large pre-strain cases, respectively. Some specimens exhibit much larger increase or even decreasing trend with increasing strain. These could be due to cracks, which were formed locally in the UV-Vis interrogation beam path, or too deep wrinkles that did not flatten enough to affect the transmittance during the loading.

3.2. Sheet resistance of PEDOT:PSS at tensile strains

Sheet resistance of the corrugated PEDOT:PSS thin films shows strong relation with the number of PEDOT:PSS layers (Figure 9). Similar to the sheet resistance of the inkjet-printed PEDOT:PSS thin films reported in [22], sheet resistance of the corrugated PEDOT:PSS thin films exhibited exponential decrease with increasing number of layers. In particular, with 5 layers or more number of the corrugated PEDOT:PSS thin films showed below ~20 Ω/sq. In particular, there was negligible effect by the pre-strain while specimens with less than 5 layers are affected more by the pre-strain. It is because the wrinkle profiles of the corrugated PEDOT:PSS thin films with less than 5 layers

Preprints (www.preprints.org) | NOT PEER-REVIEWED | Posted: 10 September 2018 doi:10.20944/preprints201809.0154.v1

Peer-reviewed version available at *Materials* **2018**, *11*, 1970; doi:10.3390/ma11101970

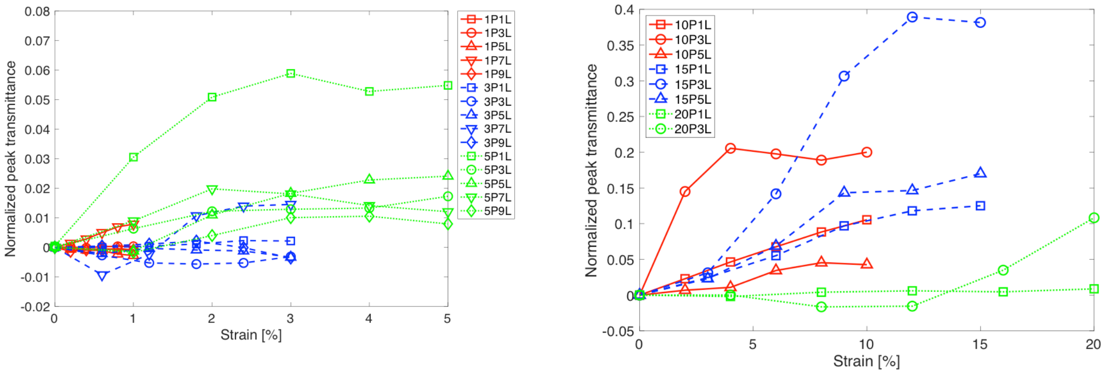

(a) (b)

Figure 8. Normalized maximum transmittance change is shown with applied strain for the corrugated PEDOT:PSS thin film specimens, which were fabricated at (a) low pre-strain up to 5% and (b) high pre-strain up to 20%.

change more drastically with the pre-strain due to smaller critical buckling strain than PEDOT:PSS thin films with more than 5 layers. Sheet resistance change of the corrugated PEDOT:PSS thin film with 1 layer largest decrease with increasing pre-strain. This is due to the longer actual length of the PEDOT:PSS thin film than the distance between electrodes in the specimen at higher pre-strain. The corrugated thin film's actual length, which is contoured along the wrinkled thin films, is longer than the length directly measured between two points (*i.e.*, two electrodes). It needs to be noted the sheet resistance was calculated with the shortest length between electrodes, instead of the contoured length. The higher pre-strain thin films tend to have more wrinkles and thus larger difference between the shortest length, which was used for calculation of sheet resistance, and the contoured length, which is attributed to the decrease in sheet resistance of the 1 layer specimen with increasing pre-strain.

In Figure 10, representative results on change in sheet resistance of the representative specimens are shown with tensile strain applied to the specimens. Figure 10a shows one representative results to show how sheet resistance changes with applied tensile strain for small pre-strain specimens. The 3% pre-strain specimen's sheet resistance is barely affected by the applied tensile strain. Large pre-strain specimens also show quite consistent sheet resistance up to half of the applied maximum tensile strain (Figure 10b). But, as the applied tensile strain increases more, sheet resistance increases, which seems due to formation of crack openings.

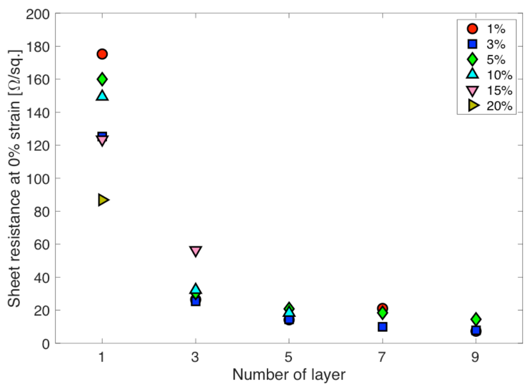

Figure 9. Sheet resistances of the corrugated PEDOT:PSS thin films exponentially decreases as the number of deposited PEDOT:PSS layer increases. Pre-strain shows effect in sheet resistance for the 1 layer case. But, it becomes weaker as the number of layers increases.

Peer-reviewed version available at Materials 2018, 11, 1970; doi:10.3390/ma11101970

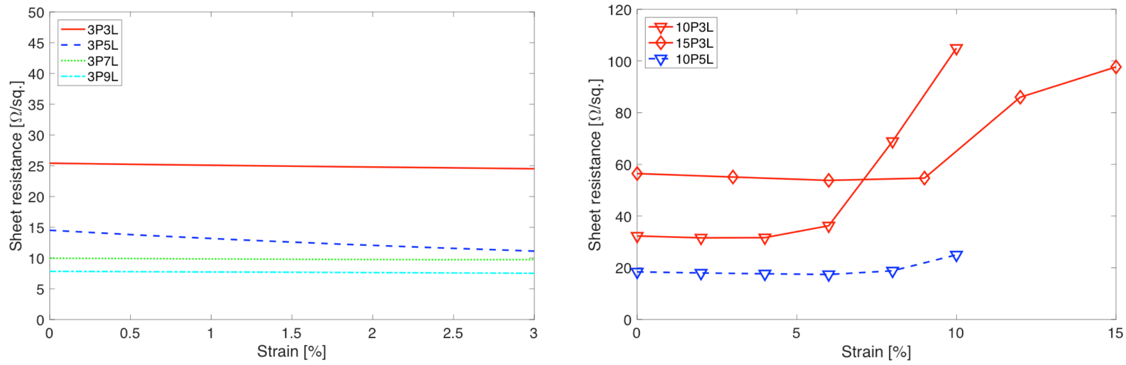

(a) (b)

Figure 10. Effect of applied tensile strain on the sheet resistance is shown for (a) the 3% pre-strain specimen and (b) high pre-strain specimens fabricated at 10% and 15% pre-strain.

3.3. Light absorption of P3HT:PCBM at tensile strains

Light absorptivity of the corrugated P3HT:PCBM thin films shows different characteristics depending on the pre-strain applied for fabrication of the corrugated thin films. In Figure 11a and b, two representative UV-Vis light absorption spectrums are shown from 3% and 15% pre-strain specimens at various tensile strains during loading cycle. The 3% pre-strain specimen show increasing light absorption with increasing tensile strain while the 15% pre-strain specimen show decreasing light absorption with increasing tensile strain. The different characteristics of the corrugated P3HT:PCBM thin films are presented in Figure 11c. The linear responses of the peak

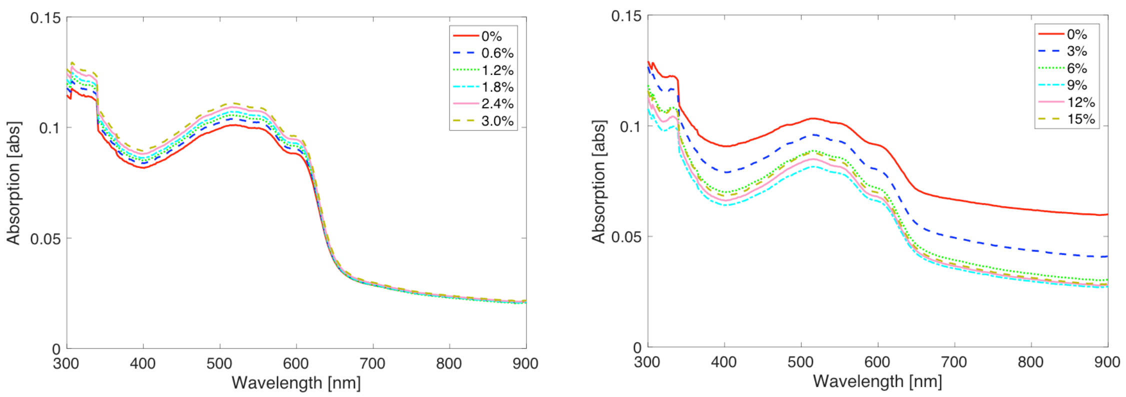

(a) (b)

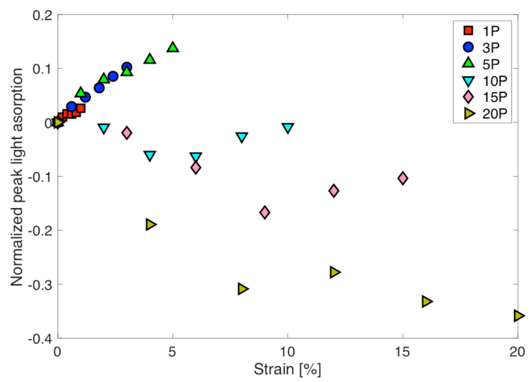

(c)

Figure 11. Light absorption spectrums of (a) 3P and (b) 15P P3HT:PCBM thin film specimens are shown at various strains from 0% to pre-strain levels, which are 3% and 15%, respectively. (c) Corrugated P3HT:PCBM thin films that are fabricated at low pre-strain are show increasing trend, while other specimens fabricated at higher pre-strain (*i.e.*, above 10%) show decreasing trend, as the applied strain increases

Preprints (www.preprints.org) | NOT PEER-REVIEWED | Posted: 10 September 2018 doi:10.20944/preprints201809.0154.v1

Peer-reviewed version available at Materials 2018, 11, 1970; doi:10.3390/ma11101970

Table 4. Strain sensitivity of the maximum light absorption of the corrugated P3HT:PCBM thin film specimens during loading cycle

Specimen # (number of layer)	P1 (1)	P3 (3)	P5 (5)
Strain sensitivity	2.61	3.41	2.74

light absorption of small pre-strain specimens are quantified by calculating strain sensitivities (Table 4) using:

$$SS_A = \frac{(A_P - A_{P,0\%})/A_{P,0\%}}{\varepsilon} \tag{3}$$

where, SS_A is strain sensitivity of peak absorption, A_P is peak absorption at a strain, $A_{P,0\%}$ is peak absorption at 0% strain, ε is applied tensile strain. The strain sensitivities are similar to the values reported from the non-corrugated P3HT:PCBM thin films [23]. One can understand that low pre-strain P3HT:PCBM thin film specimens did not form as many as wrinkles like high pre-strain P3HT:PCBM thin film specimens. But, high pre-strain P3HT:PCBM thin film specimens exhibit dramatic decrease in light absorptivity with increasing applied tensile strain up to half of maximum applied strain, which seems mainly because wrinkles become more flat at higher strain. The increasing trend of light absorption at above half of tensile strain with the applied tensile strain is thought to result from the stretch of the thin films, where P3HT molecules are aligned more, due to applied tensile strain. The continuous and most significant decrease in light absorption of the 20% specimen seems to be attributed mainly to formation of cracks in the thin films.

3.4. DC-based tensile strain sensing of flexible strain sensor

The corrugated PEDOT:PSS thin films fabricated using 7 or more number of layers exhibited lowest sheet resistance and were affected less by the pre-strain. On the other hand, the corrugated P3HT:PCBM thin films fabricated at 1%, 3%, or 5% pre-strain exhibited light absorption increasing proportionally with increasing applied tensile strain. Therefore, only six different flexible strain sensors were fabricated at 1%, 3%, or 5% pre-strain with 7 or 9 layers of corrugated PEDOT:PSS thin films. To validate the performance of radiant-electric energy conversion performance of the fabricated flexible strain sensor, current-voltage (IV) responses were obtained. One representative set of dark and light IV response is shown in Figure 12 for the flexible strain sensor fabricated using 1 layer of corrugated P3HT:PCBM thin film and 7 layers of the corrugated PEDOT:PSS thin films, which are fabricated at 1% pre-strain. Figure 12 inset shows short circuit current (*i.e.*, y-intercept) and open circuit voltage (*i.e.*, x-intercept), which are ~2.5 μA and 0.05 V, respectively.

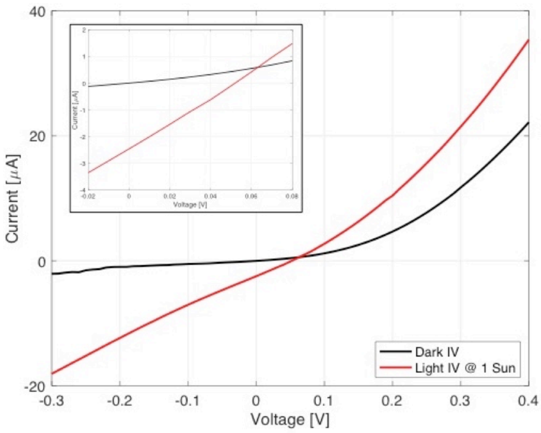

Figure 12. Current-voltage response of FS-1P7L specimen is shown under one-sun light and without light. In the inset, short circuit current and open circuit voltage are shown closely from the vertical axis intercept and the horizontal axis intercept.

Peer-reviewed version available at Materials 2018, 11, 1970; doi:10.3390/ma11101970

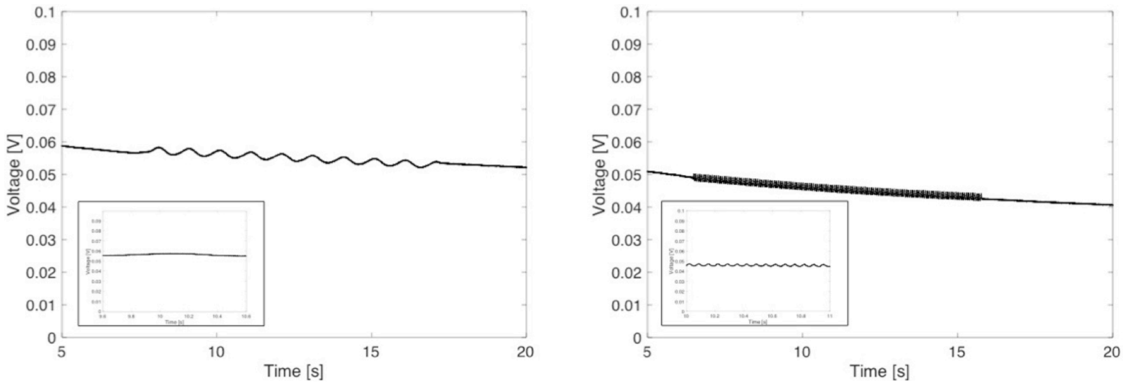

(a) (b)

Figure 13. DC voltage responds to tensile loading and unloading cycles applied to FS-1P7L from 0% to 1% at (a) 1 Hz and (b) 15 Hz. Inset plots show the DC voltage response during 1 s time duration.

Figure 13 shows DC voltage response generated from the FS-1P7L flexible strain sensors in time domain when the strain sensor was subjected to sinusoidal tensile strain loading and unloading cycles. As the loading frequency increases from 1 Hz to 15 Hz while maintaining minimum and maximum tensile strains consistent, cycles of the generated DC voltage also shifts its frequency from 1 Hz to 15 Hz. DC voltage generated from the 1% pre-strain sensors (*i.e.*, FS-1P7L and FS-1P9L) responds very well to the applied sinusoidal tensile strain loading and unloading cycles. Other four sensor specimens, which are fabricated at higher than 1% pre-strain, produced sensor signal with low signal-to-noise ratio. It is thought to be mainly due to disturbance in liquid EGaIn electrodes.

In Figure 14a, the normalized DC voltage of FS-1P7L is presented with the applied load pattern at 5 Hz. Although there is slight decay in DC voltage signal, it can be clearly seen that overall DC voltage sensor responds to the applied load pattern very well. Figure 14b shows how strain sensitivity of the 1% pre-strain flexible sensor specimens, which exhibited strain sensing capability with high signal-to-noise ratio, changes with the loading frequency of the applied tensile loading and unloading cycles. Strain sensitivities of the 1% pre-strain specimens are higher than the ones of light absorption-based strain sensitivities. The higher DC voltage-based strain sensitivity seems due to the strain sensitivity light transmittance of the corrugated PEDOT:PSS thin films. It should be noted that the light transmittance of the corrugated PEDOT:PSS thin films increased as the applied tensile strain increased, which allows more photons to pass through the PEDOT:PSS thin films to be absorbed by the P3HT:PCBM thin films.

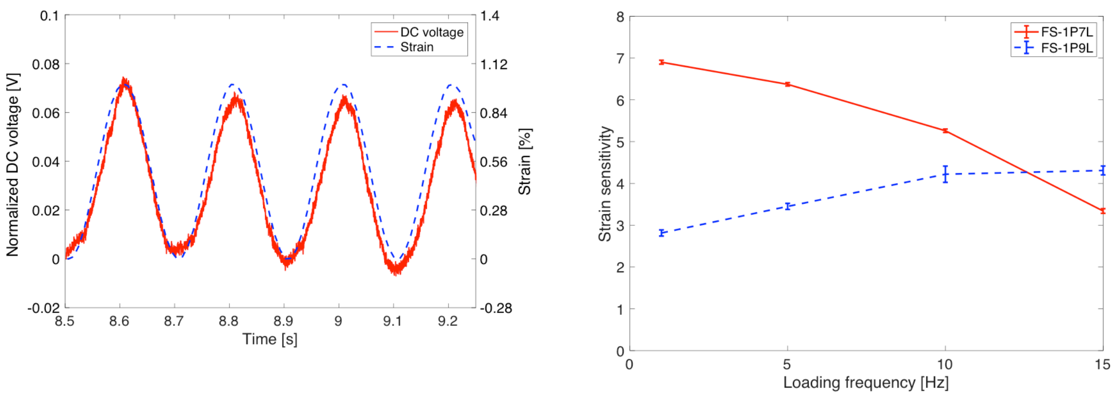

(a) (b)

Figure 14. (a) DC voltage generated from FS 1P7L sensor specimen varies with applied sinusoidal tensile loading and unloading cycles. (b) Strain sensitivities of the flexible sensor specimens are shown with change of loading frequency.

Preprints (www.preprints.org) | NOT PEER-REVIEWED | Posted: 10 September 2018 doi:10.20944/preprints201809.0154.v1

Peer-reviewed version available at Materials 2018, 11, 1970; doi:10.3390/ma11101970

4. Conclusions

In this study, a flexible strain sensor is designed using corrugated multilayered thin films using P3HT and PEDOT:PSS. The flexible strain sensor generated DC voltage under one-sun light from the solar simulator, and the DC voltage magnitude was shown to vary with the applied tensile strain up to 5% tensile strain. To make the DC voltage-based strain sensor mechanically resilient and exhibit wide strain sensing range, thin film buckling was intentionally induced by pre-straining the PDMS substrates, where the multilayered thin films are deposited on, during fabrication process and released afterwards. As a result, best performance of the flexible strain sensor was achieved at 1% pre-strain with highest gage factor (*i.e.*, 7) among the fabricated flexible strain sensors and highest signal-to-noise ratio. Other flexible sensors fabricated at 3% and 5% also exhibited DC voltage-based strain sensing capability but with low signal-to-noise ratio.

In addition, the functional thin film constituents of the flexible strain sensor were characterized by measuring optical properties and electrical properties. First, the corrugated PEDOT:PSS thin films' light transmittance and sheet resistance were studied with various fabrication design parameters (*i.e.*, pre-strain and the number of PEDOT:PSS layer). It was shown that the corrugated PEDOT:PSS thin film's optical transmittance is affected by both fabrication design parameters. Higher transmittance was acquired at lower pre-strain due to less populated wrinkles with shallower depths. As the number of layer (*i.e.*, thickness) increases, decreasing trend was observed in light transmittance. Yet, lowest sheet resistance was achieved at 7 or 9 layers of PEDOT:PSS thin film. In addition, the sheet resistance of the corrugated thin films was less affected by applied tensile strain at low pre-strain regardless of the number of layers. Second, the corrugated P3HT:PCBM self-sensing thin films exhibited increasing peak light absorption trend at low pre-strain with increasing applied tensile strain while higher pre-strain specimens showed opposite trend. This provided a design guideline for the corrugated PEDOT:PSS thin films for fabrication of flexible strain sensor to be fabricated using 7 or 9 layers of corrugated PEDOT:PSS thin films and 1 layer of corrugated P3HT:PCBM thin films at 5% or smaller pre-strain.

Acknowledgments: Authors would like to thank Dr. Bhaskar Majumdar to generously allow A.M. to use the MTS load frame and an optical microscope.

Author Contributions: D.R. conceptualized the work, planned the research activities, supervised the project progresses, performed data analysis, and wrote manuscript; A.M. performed experimentations and experimental data processing.

Funding: This research is supported by NASA EPSCoR CAN (grant #: 80NSSC17M0050), New Mexico Space Grant Consortium, and NASA's Space Grant College and Fellowship Program.

Conflicts of Interest: The authors declare no conflict of interest.

5. References

1. Do Hoon, L.; Jonghyurk, P.; Jong-Kwon, L.; Kwang, H.; Dong-Jin, L.; Ye Rim, L.; Byung Yang, L. Highly sensitive and flexible strain sensors based on patterned ito nanoparticle channels. *Nanotechnology* **2017**, *28*, 495501.
2. Ryu, D.; Loh, K.J.; Ireland, R.; Karimzada, M.; Yaghmaie, F.; Gusman, A.M. In situ reduction of gold nanoparticles in pdms matrices and applications for large strain sensing. *Smart Structures and Systems* **2011**, *8*, 471-486.
3. Han, F.; Li, J.; Zhao, S.; Zhang, Y.; Huang, W.; Zhang, G.; Sun, R.; Wong, C.-P. A crack-based nickel@graphene-wrapped polyurethane sponge ternary hybrid obtained by electrodeposition for highly sensitive wearable strain sensors. *Journal of Materials Chemistry C* **2017**, *5*, 10167-10175.
4. Jang, S.-H.; Park, Y.-L.; Yin, H. Influence of coalescence on the anisotropic mechanical and electrical properties of nickel powder/polydimethylsiloxane composites. *Materials* **2016**, *9*, 239.
5. Laflamme, S.; Kollosche, M.; Connor, J.; Kofod, G. Robust flexible capacitive surface sensor for structural health monitoring applications. *Journal of Engineering Mechanics* **2013**, *139*, 879-885.
6. Wang, Y.; Yang, R.; Shi, Z.; Zhang, L.; Shi, D.; Wang, E.; Zhang, G. Super-elastic graphene ripples for flexible strain sensors. *ACS Nano* **2011**, *5*, 3645-3650.
7. Xian, H.; Cao, C.; Shi, J.; Zhu, X.; Hu, Y.; Huang, Y.; Meng, S.; Gu, L.; Liu, Y.; Bai, H. Flexible strain sensors with high performance based on metallic glass thin film. *Applied Physics Letters* **2017**, *111*, 121906.
8. Li, X.; Zhang, R.; Yu, W.; Wang, K.; Wei, J.; Wu, D.; Cao, A.; Li, Z.; Cheng, Y.; Zheng, Q., *et al.* Stretchable and highly sensitive graphene-on-polymer strain sensors. *Scientific Reports* **2012**, *2*, 870.
9. Someya, T.; Kato, Y.; Sekitani, T.; Iba, S.; Noguchi, Y.; Murase, Y.; Kawaguchi, H.; Sakurai, T. Conformable, flexible, large-area networks of pressure and thermal sensors with organic transistor active matrixes. *P Natl Acad Sci USA* **2005**, *102*, 12321.
10. Ryu, D.; Castaño, N.; Bhakta, R.; Kimberley, J. Fracto-mechanoluminescent light emission of eud4tea-pdms composites subjected to high strain-rate compressiveloading. *Smart Materials and Structures* **2017**.
11. Pulliam, E.; Hoover, G.; Ryu, D. Multifunctional mechano-luminescent-optoelectronic composites for self-powered strain sensing. In *ASME 2017 Conference on Smart Materials, Adaptive Structures and Intelligent Systems*, ASME: Snowbird, UT, 2017.
12. Zhou, J.; Gu, Y.; Fei, P.; Mai, W.; Gao, Y.; Yang, R.; Bao, G.; Wang, Z.L. Flexible piezotronic strain sensor. *Nano Letters* **2008**, *8*, 3035-3040.
13. Gullapalli, H.; Vemuru, V.S.M.; Kumar, A.; Botello-Mendez, A.; Vajtai, R.; Terrones, M.; Nagarajaiah, S.; Ajayan, P.M. Flexible piezoelectric zno–paper nanocomposite strain sensor. *Small* **2010**, *6*, 1641-1646.
14. Xu, S.; Yeh, Y.-w.; Poirier, G.; McAlpine, M.C.; Register, R.A.; Yao, N. Flexible piezoelectric pmn–pt nanowire-based nanocomposite and device. *Nano Letters* **2013**, *13*, 2393-2398.
15. Ryu, D.; Castaño, N. Multivariate characterization of light emission from zns:Cu-pdms self-sensing composites under cyclic tensile strains. *IEEE Sensors Letters* **2018**, *2*, 1-4.
16. Holguin, B.; Allison, J.; Ryu, D.; Alvarez, Z.; Hernandez, F.; Kimberley, J. Development of 3d impact self-sensing composites using fracto-mechanoluminescent eud4tea. In *ASME 2017 Conference on Smart Materials, Adaptive Structures and Intelligent Systems*, ASME: Snowbird, UT, 2017 (Accepted).
17. Krishnan, S.; Walt, H.V.d.; Venkatesh, V.; Sundaresan, V.B. Dynamic characterization of elastico-mechanoluminescence towards structural health monitoring. *Journal of Intelligent Material Systems and Structures* **2017**, *28*, 2458-2464.
18. Jeong, S.M.; Song, S.; Joo, K.-I.; Kim, J.; Hwang, S.-H.; Jeong, J.; Kim, H. Bright, wind-driven white mechanoluminescence from zinc sulphide microparticles embedded in a polydimethylsiloxane elastomer. *Energy & Environmental Science* **2014**, *7*, 3338-3346.
19. Laflamme, S.; Kollosche, M.; Connor, J.J.; Kofod, G. Robust flexible capacitive surface sensor for structural health monitoring applications. *Journal of Engineering Mechanics* **2013**, *139*, 879-885.
20. Pulliam, E.; Hoover, G.; Tiparti, D.; Ryu, D. In *Development of self-powered strain sensor using mechano-luminescent zns:Cu and mechano-optoelectronic p3ht*, SPIE Smart Structures and Materials + Nondestructive Evaluation and Health Monitoring, 2017; SPIE: p 15.
21. Ryu, D.; Loh, K.J. Strain sensing using photocurrent generated by photoactive p3ht-based nanocomposites. *Smart Materials and Structures* **2012**, *21*, 065016.

22. Ryu, D.; Meyers, F.N.; Loh, K.J. Inkjet-printed, flexible, and photoactive thin film strain sensors. *Journal of Intelligent Material Systems and Structures* **2015**, *26*, 1699-1710.
23. Ryu, D.; Loh, K.J. Multi-modal sensing using photoactive thin films. *Smart Materials and Structures* **2014**, *23*, 085011.
24. Ryu, D.; Meyers, F.N.; Loh, K.J. Inkjet-printed, flexible, and photoactive thin film strain sensors. *Journal of Intelligent Material Systems and Structures* **2014**.